Paper review

mainly refer to

Investigating Axisymmetric and Asymmetric Signals of Secondary Eyewall Formation Using Observations-Based Modeling of the Tropical Cyclone Boundary Layer

Chau-Lam Yu, Anthony C. Didlake Jr., Jeffrey D. Kepert, Fuqing Zhang

Wei-Ting Fang

2022.11.15 @CPLab

Outline

► **Introduction**

► **Data and Methodology**
  ► The K18(Kepert 2018) Model
  ► Tangential Wind Composite From WD18(Wunsch and Didlake 2018)
  ► Axisymmetric and Asymmetric Forcing for the K18 Model

► **Results**
  ► Axisymmetric Response
  ► Asymmetric Response
    ► Asymmetric Simulation of the Pre-SEF Group
    ► Quadrant-Averaged Analysis of the Pre-SEF Group
    ► Quadrant-Averaged Analysis of the Non-SEF and Post-SEF Groups
  ► Sensitivity Analysis of Updraft Variability
    ► Bootstrapping Analysis of the Outer Updraft Strength
    ► Variability of the Boundary Layer Response in Pre-SEF Ensemble

► **Discussion and conclusions**

Introduction(1/2)

► Previous studies have hypothesized that certain dynamical features are important for SEF, including outward-propagating vortex-Rossby waves (VRWs) (Guimond et al., 2020; Menelaou et al., 2012; Montgomery & Kallenbach, 1997), convectively generated potential vorticity anomalies from inward-spiraling rainbands (Judt & Chen, 2010; Qiu et al., 2010), an enhanced background vorticity radial gradient (Abarca & Corbosiero, 2011; Terwey & Montgomery, 2008), and a region of rapid filamentation that supports the formation of a precipitation-free moat outside a primary eyewall (Rozoff et al., 2006; H. Wang et al., 2019; Y. Wang, 2008).

► Several studies have shown that SEF occurs in association with the development of enhanced supergradient flow in the upper boundary layer (Abarca & Montgomery, 2013, 2014; Abarca et al., 2015; Huang et al., 2012; Wu et al., 2012).

► Many of the previously mentioned theories require some pre-existing vorticity anomaly outside of the eyewall to modulate or initiate a certain axisymmetric dynamical mechanism, where this vorticity anomaly is generated by rainband convection. On the other hand, the VRW SEF theory does not require such pre-existing rainband convection, but rather the source of vorticity comes from the inner core in the form of outward-propagating filaments (convectively coupled VRWs), as discussed by Fischer et al. (2020) and Guimond et al. (2020).

Introduction(2/2)

► Wunsch and Didlake (2018, hereafter WD18) examined SEF in a composite analysis of aircraft 700 hPa level observations from 17 yr of Atlantic basin TCs. They showed that storms prior to SEF exhibited an axisymmetric broadening of the outer tangential wind field. This broadened wind field has commonly been identified as a precursor to SEF in observational studies (Bell et al., 2012; Didlake & Houze, 2013; Sitkowski et al., 2011) and modeling studies (Rozoff et al., 2006, 2012; Sun et al., 2013; Tang et al., 2017; Wang et al., 2016, 2019).

► Furthermore, WD18 showed that storms prior to SEF experience the largest change of the tangential wind field in the storm quadrants left of the 850–200 hPa environmental wind shear vector. This finding aligns with previous studies identifying a mesoscale descending inflow (MDI) pattern in left-of-shear stratiform rainbands that locally accelerates the tangential wind field prior to SEF (Didlake & Houze, 2013; Didlake et al., 2018; Yu et al., 2021).

► Building upon the results from WD18 and other previous studies, this study uses the K18 model to examine the steady-state boundary layer response to the tropospheric forcing represented by the observational composites of WD18. Both axisymmetric mean and asymmetric forcings are used to investigate how the boundary layer responds to the free tropospheric forcing aloft during SEF events and within storms without SEF.
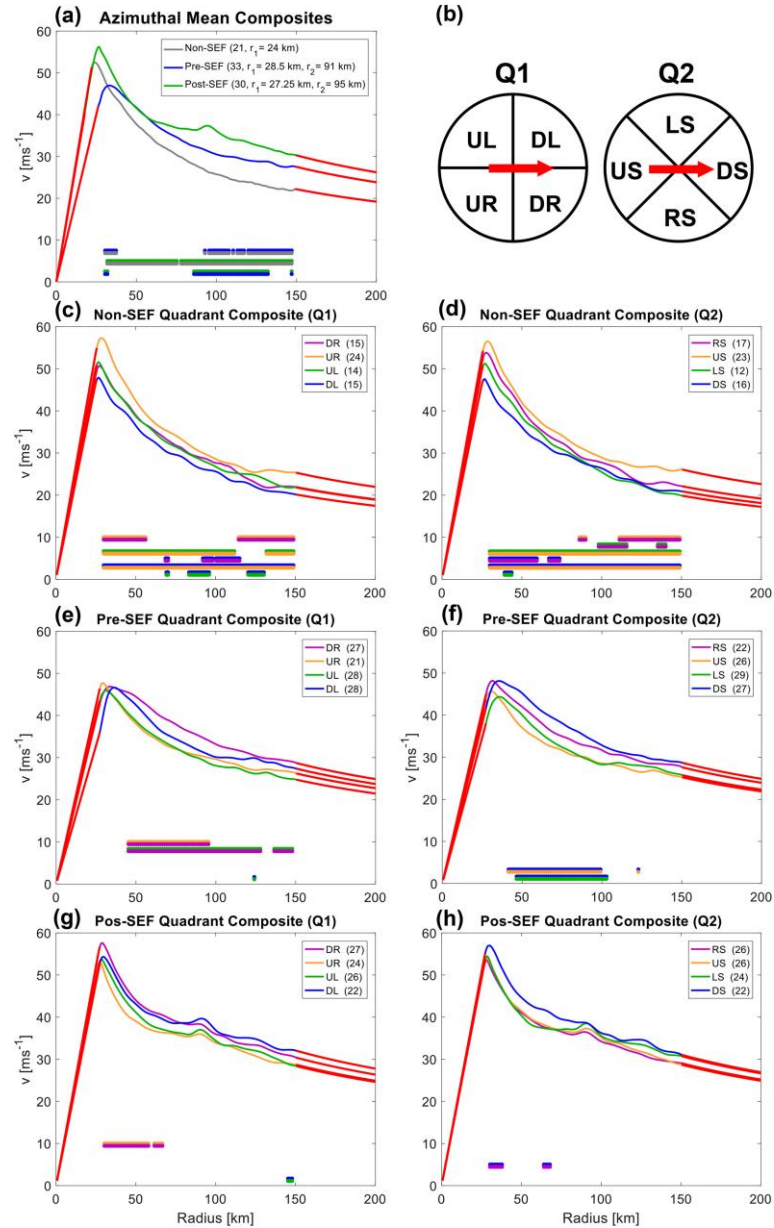
The K18 Model

► Nonlinear boundary layer model developed by Kepert and Wang (2001) and later modified by Kepert (2018, the K18 model).

  ► simulates the steady-state boundary layer response by integrating a set of prognostic three-dimensional nonlinear primitive equations to a near steady state.

► The model is dry and is forced by the pressure forcing from the free-tropospheric wind at the top of the integration domain, which is assumed to be above the boundary layer and is held constant in time.

► Since no feedback to the forcing field is included in the model, the simulated response is a one-way response of the boundary layer to the free tropospheric forcing. This simulated response includes boundary layer updrafts that are purely driven by frictional convergence. If moist processes were included in this same model, we would expect that the additional buoyancy effects would produce stronger updrafts.

► Different from the axisymmetric KW01 model, the pressure forcing used in the K18 model top can be either axisymmetric or asymmetric.

► When axisymmetric forcing is used, the simulated result is equivalent to the KW01 model. When asymmetric forcing is used, it allows the investigation of the boundary layer response to cyclone asymmetries induced by environmental influences, such as environmental wind shear.

► This pressure forcing is implicitly represented by the gradient wind assumption in the axisymmetric mode and by a nondivergent wind in the asymmetric case through a nonlinear balance relation.

► Following the recommendation of Kepert (2012), the neutral Louis boundary layer scheme is used in the K18 model to parameterize momentum diffusion.

► The model has 20 vertical levels, covering from 10 m near the surface to 2.25 km. The maximum vertical spacing is 200 m and the horizontal grid spacing is 3 km. All experiments are integrated for 48 h to a nearly steady state.
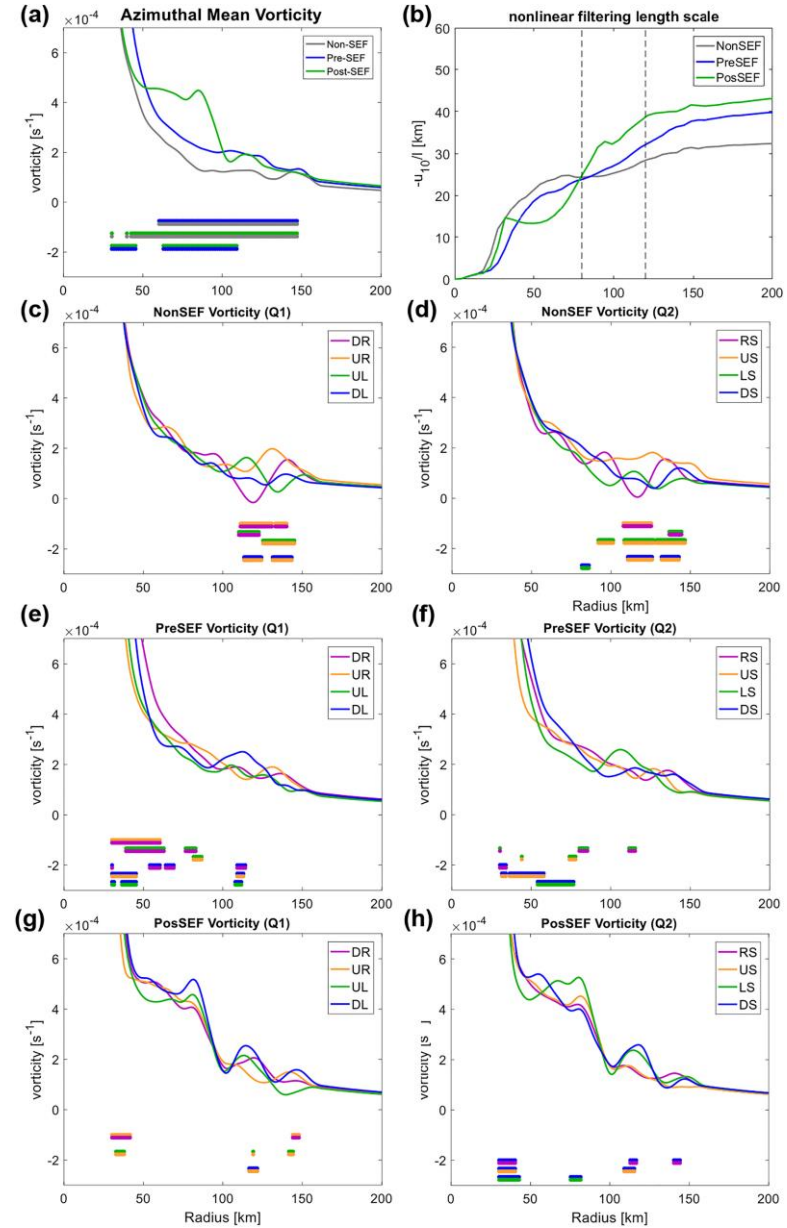
Tangential Wind Composite From WD18

► WD18 used the Extended Flight-Level Data set for TCs (FLIGHT+; Vigh et al., 2016) to perform a composite analysis for Atlantic hurricanes at category 3 (49.6 m s^{-1} maximum winds) or higher from year 1999 to 2015.

► The 700 hPa level flight legs are then selected, and divided into groups without, prior to, and after SEF (the "Non-SEF," "Pre-SEF," and "Post-SEF" groups).

► For the "Non-SEF" group, the wind profiles are normalized by the radius of maximum wind (r_1, RMW).

► For the Pre-SEF and Post-SEF groups, the flight legs were normalized by two length scales. For radii less than the RMW, the wind profile was normalized by the RMW (r_1), while outside the RMW, the wind profile was normalized by the width of the moat (m), which is defined as the distance between the primary and secondary tangential wind maxima in the observed tangential wind profiles. The radius of the secondary maximum wind (r_2) is equal to $m+r_1$.
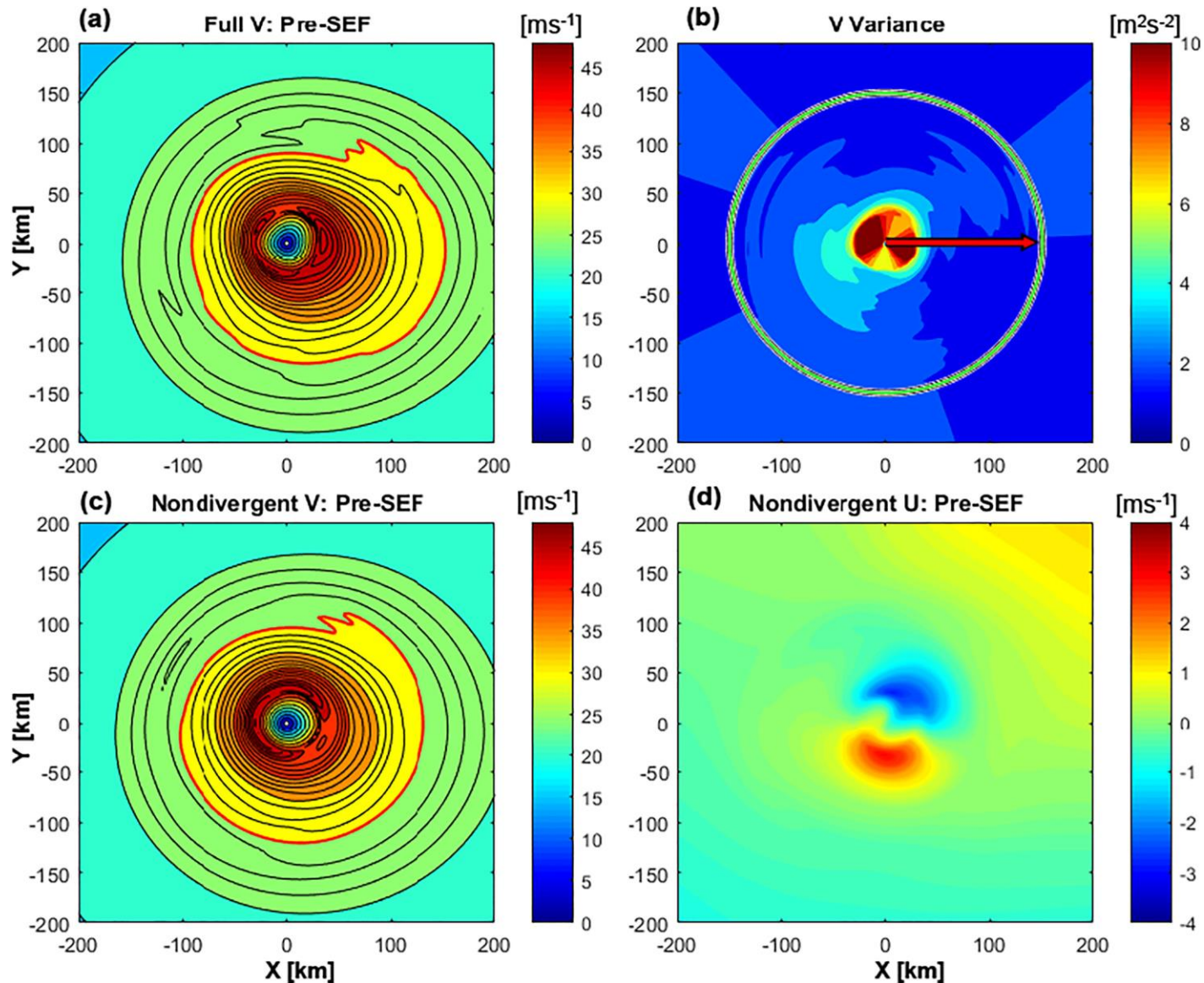
Azimuthal composite profiles

Asymmetric forcing

(a) Full V: Pre-SEF [ms⁻¹]

(b) V Variance [m²s⁻²]

(c) Nondivergent V: Pre-SEF [ms⁻¹]

(d) Nondivergent U: Pre-SEF [ms⁻¹]

Smoothed asymmetric nondivergent wind:

$$v_{\psi} = \left(\partial\psi / \partial r, -1 / r\partial\psi / \partial\lambda \right)$$

It can be shown that the solution of the optimal interpolation is also the solution of the following generalized Poisson equation:

$$\frac{1}{r}\frac{\partial}{\partial r}\left(r\left(\frac{1}{\sigma_o^2} \right)\frac{\partial\psi}{\partial r} \right) + \frac{1}{r^2}\frac{\partial}{\partial\lambda}\left(\frac{1}{\sigma_B^2}\frac{\partial\psi}{\partial\lambda} \right) = \frac{1}{r}\frac{\partial}{\partial r}\left(r\left(\frac{v_o}{\sigma_o^2} \right) \right)$$

Axisymmetric Response

(a) NonSEF axisymmetric simulation: u, w
(d) PreSEF axisymmetric simulation: u, w
(g) PosSEF axisymmetric simulation: u, w
(b) NonSEF axisymmetric simulation: v, v jet
(e) PreSEF axisymmetric simulation: v, v jet
(h) PosSEF axisymmetric simulation: v, v jet
(c) NonSEF axisymmetric simulation: u, div
(f) PreSEF axisymmetric simulation: u, div
(i) PosSEF axisymmetric simulation: u, div
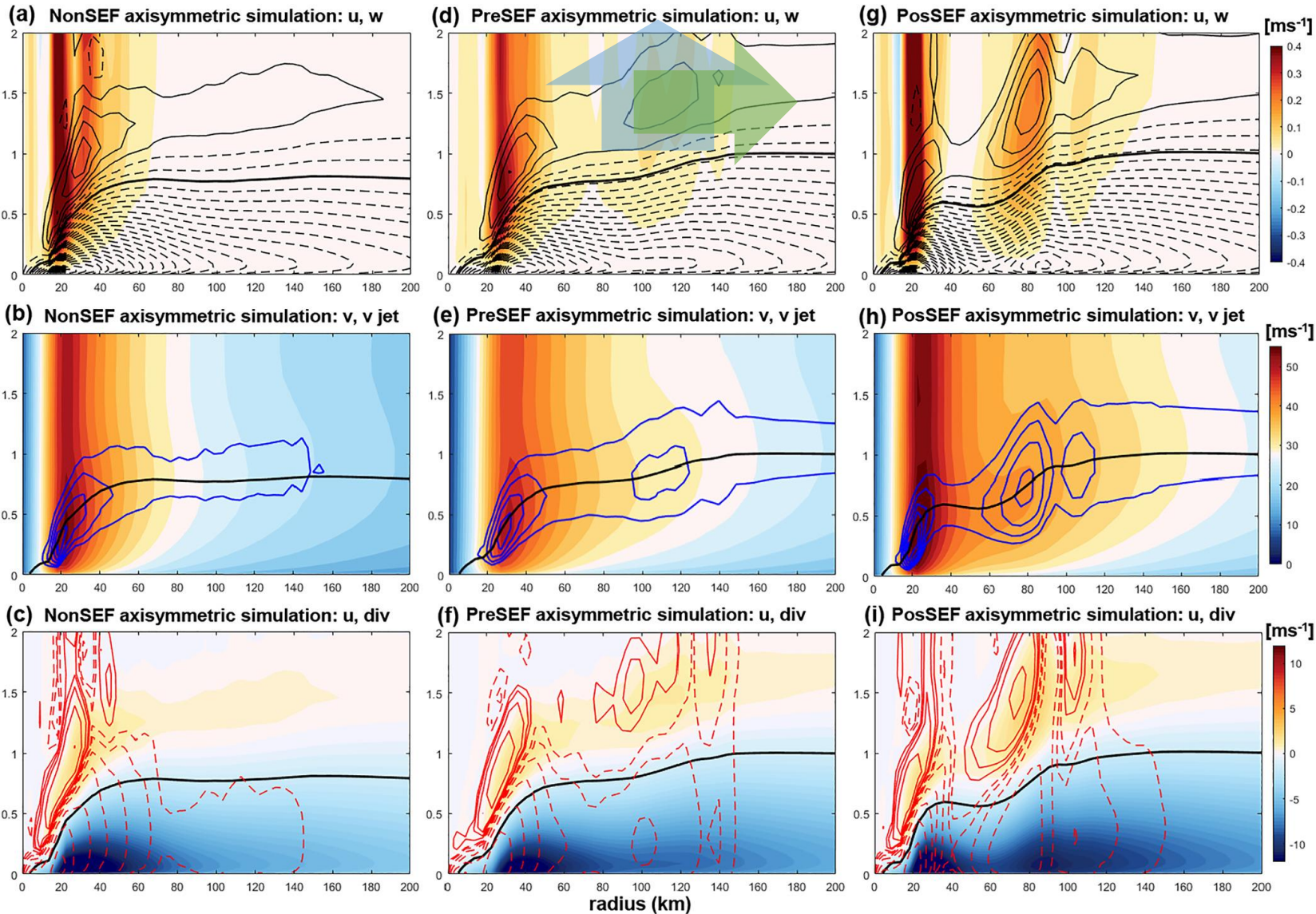
The boundary layer depth (as approximated by the height of 10% peak radial inflow) varies between 0.5 and 1 km outside the eyewall and out to 200 km radius. These depths are slightly lower than those found in the observations-based axisymmetric composites from J. A. Zhang et al. (2011), but these are still realistic depths that fall within the range of observed boundary layer depths (Kepert et al., 2016; J. A. Zhang et al., 2013).

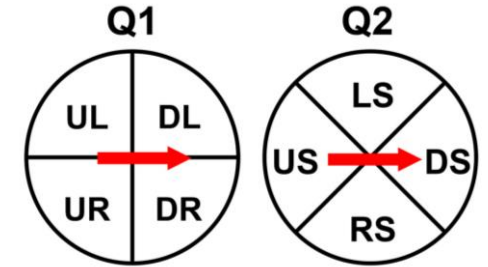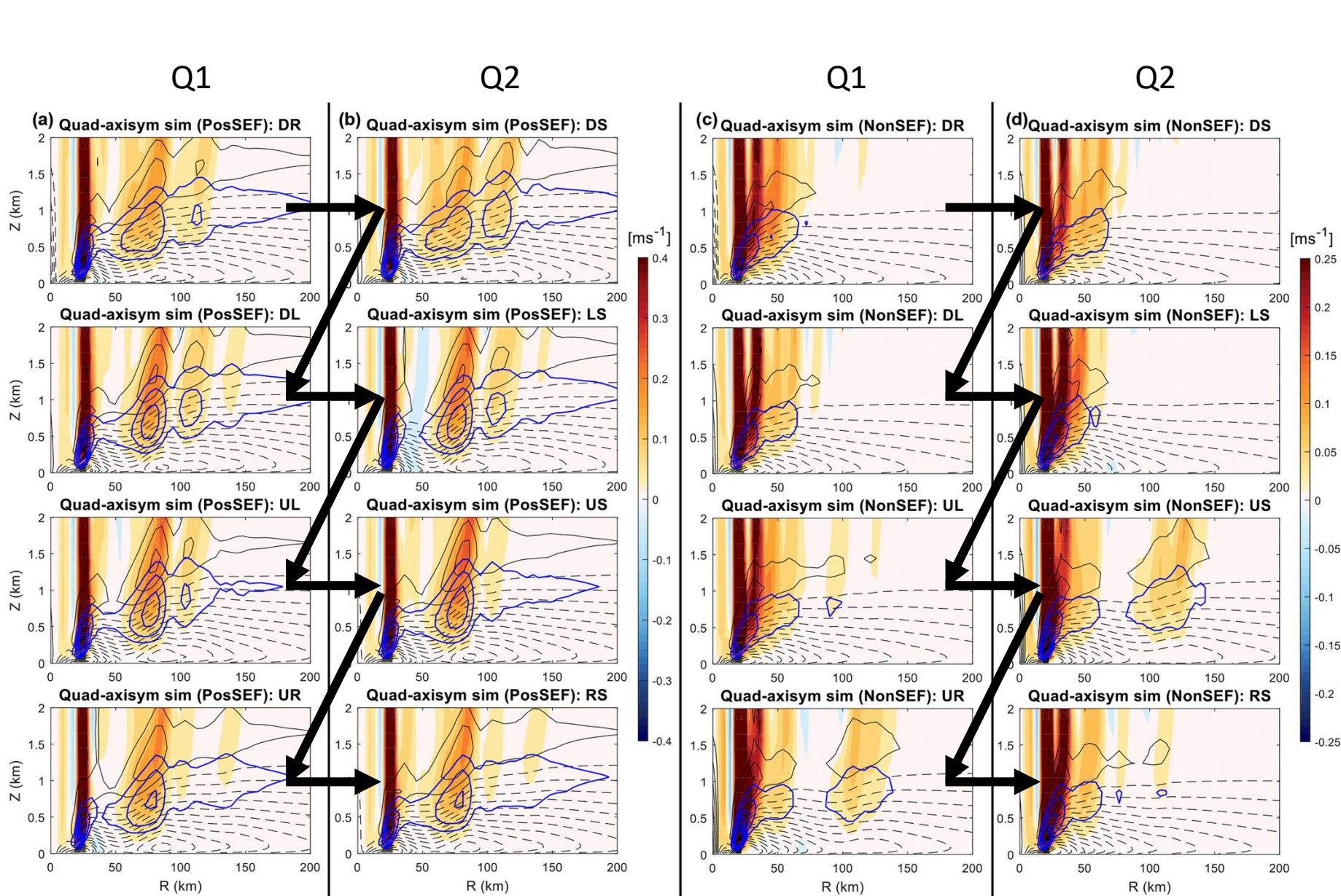# Asymmetric Simulation of the Pre-SEF Group
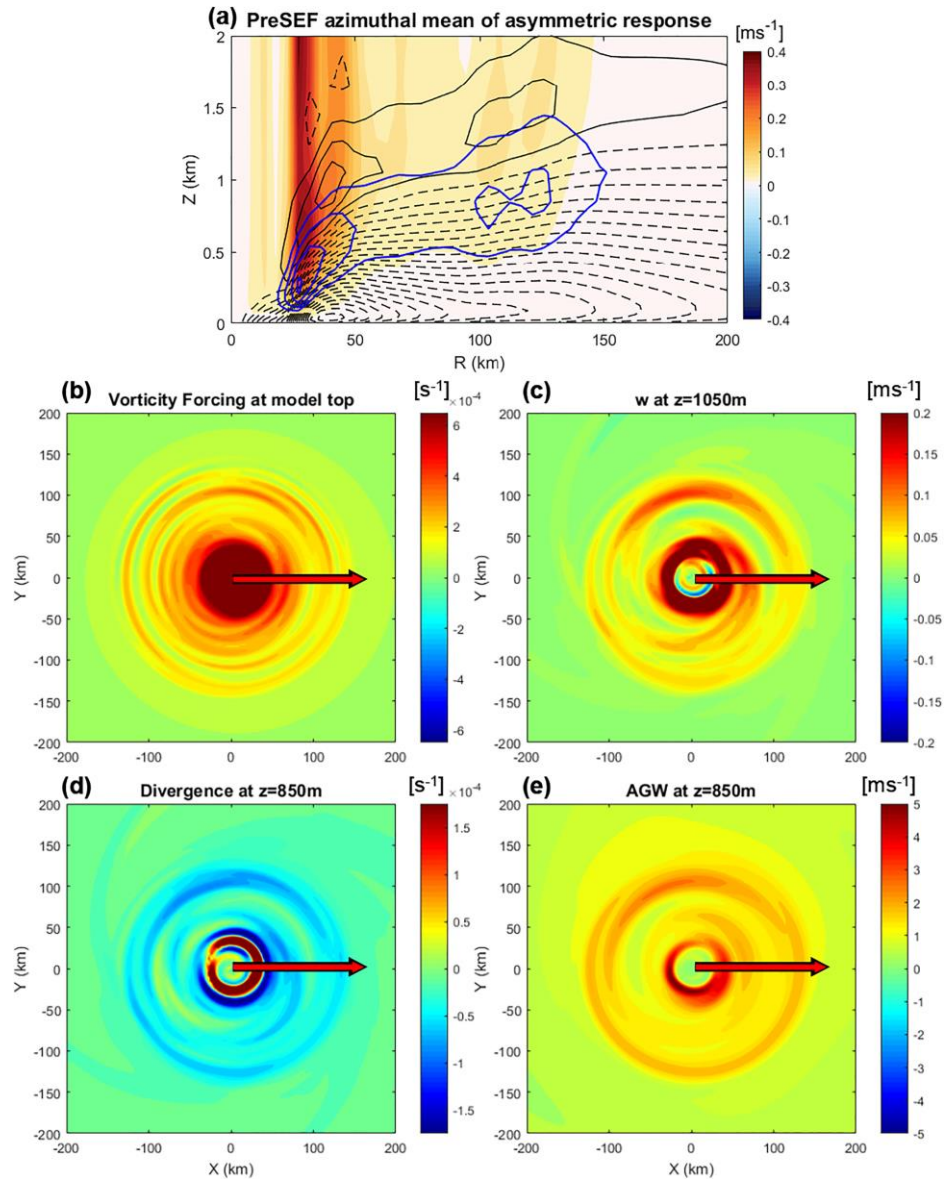
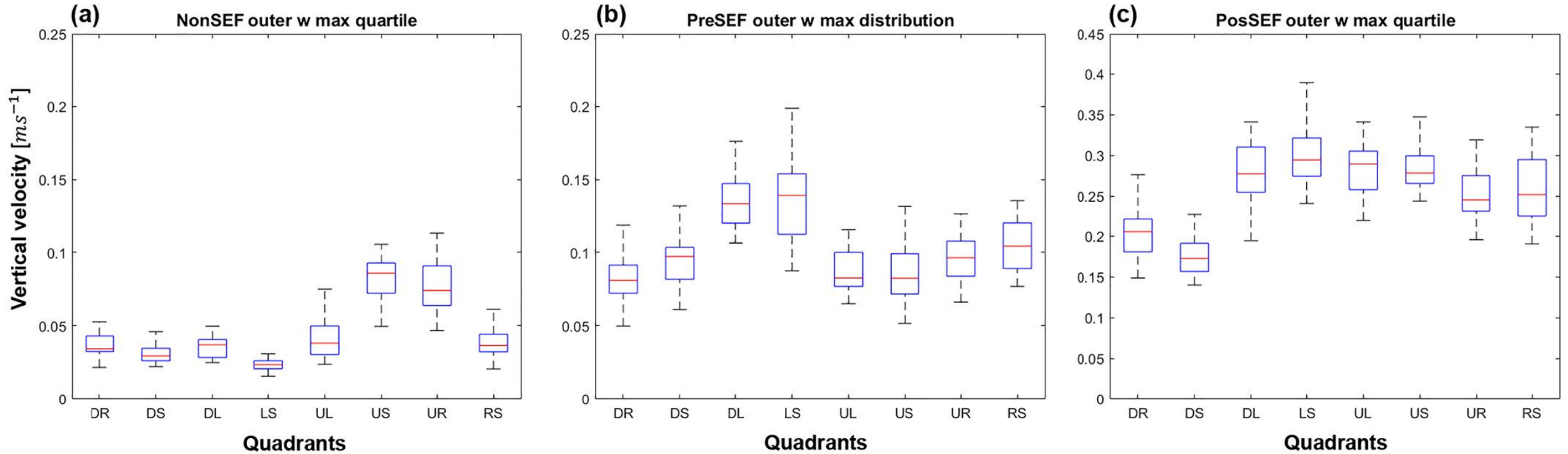# Quadrant-Averaged Analysis of the Pre-SEF Group
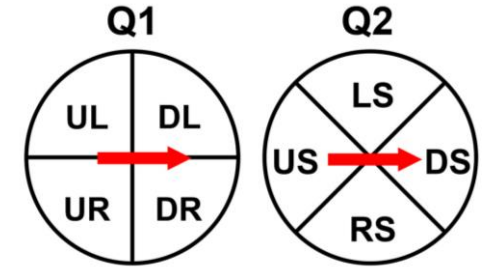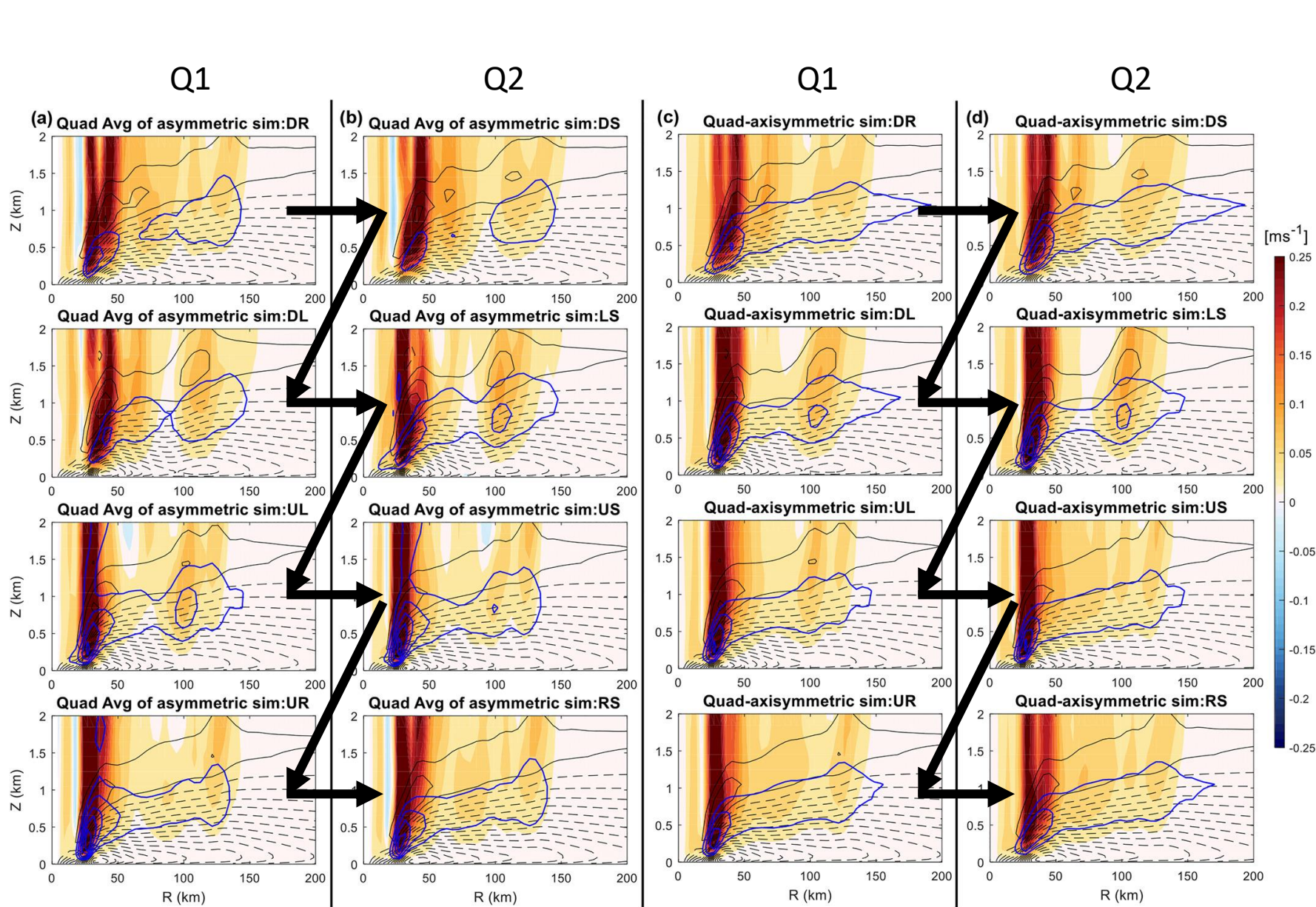
Both the supergradient wind and radial outflow maxima exhibit a noticeable downwind shift compared to the azimuthal locations of the updraft and boundary layer inflow maxima.

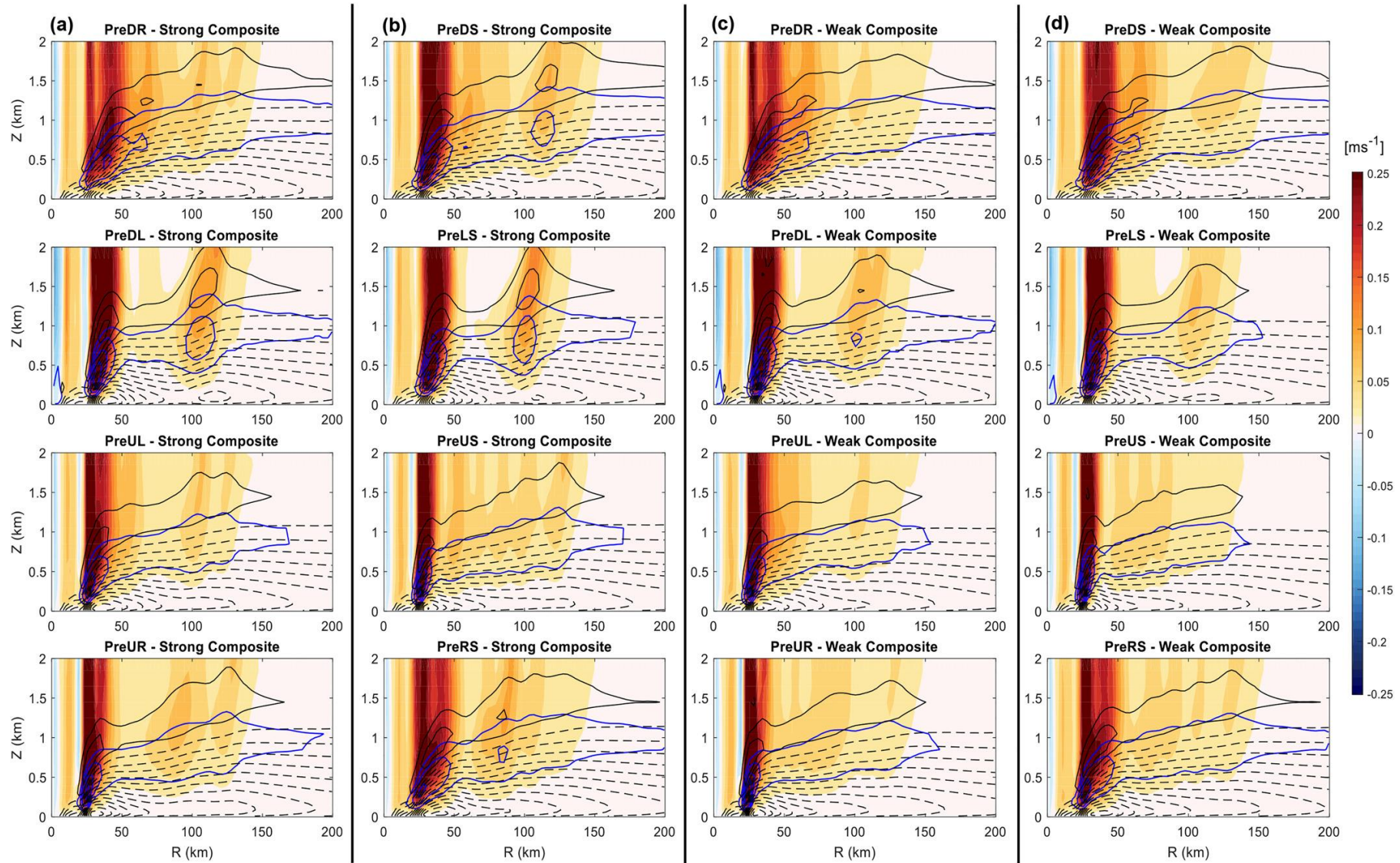# Quadrant-Averaged Analysis of the Non-SEF and Post-SEF Groups

Bootstrapping Analysis of the Outer Updraft Strength

The maximum outer updraft is defined as the maximum value of the vertical velocity between 90 and 140 km radial range.

Discussion and Conclusions (1/2)

► In this study, we examined the TC boundary layer response to imposed free-tropospheric forcing derived from observations to investigate the axisymmetric and asymmetric boundary layer response during SEF.

► Observed tangential wind composite profiles of storms without SEF, prior to SEF, and after SEF (Non-, Pre-, and Post-SEF; Wunsch & Didlake, 2018) are used to the force the Kepert (2018) diagnostic boundary layer model (the K18 model), which is integrated for 48 h to examine the steady-state boundary layer response to the tropospheric forcing.

► The asymmetric wind field displayed a broadened tangential wind field and an enhanced vorticity band in the downshear and left-of-shear regions. The simulated boundary layer response had a clear band of outer updraft and strengthened boundary layer inflow, corresponding to the vorticity band in the asymmetric wind field, primarily in the left-of-shear quadrants.

► Our results indicate that the strongest signal is indeed in the DL and LS quadrants of the Pre-SEF group, which is driven largely by the vorticity structure of the broadened tangential wind field in these quadrants.

Discussion and Conclusions (2/2)

▶ Yu et al. (2021) showed that the mesoscale descending inflow in the left-of-shear stratiform precipitation region was accompanied by inward advection of angular momentum, which preceded the emergence of a sustained low-level updraft in the left-of-shear regions.

▶ It remains possible that VRWs in the left-of-shear quadrants led to acceleration of the left-of-shear tangential winds and thus enhanced local vorticity, as described by Guimond et al. (2020).

▶ It also remains possible that VRWs led to a direct spin-up of the axisymmetric secondary tangential wind maximum in our SEF cases (Fischer et al., 2020; Guimond et al., 2020; Montgomery & Kallenbach, 1997).

▶ Distinct from direct spin-up mechanisms, the axisymmetrization of the observed left-of-shear features also remains a possible factor via previously proposed axisymmetrization theories (e.g., Abarca & Montgomery, 2013; Huang et al., 2012; Kepert, 2013; Kepert & Nolan, 2014; Miyamoto et al., 2018; Rozoff et al., 2006; Y. Wang, 2008).